Desalination 593 (2025) 118198

Contents lists available at ScienceDirect

Desalination

journal homepage: www.elsevier.com/locate/desal

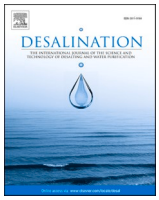

A perspective on MXene-enhanced biofiltration-membrane water reuse treatment systems: A review and experimental validation

Mostafa Dadashi Firouzjaei [a,b,c,e,*], Jonathan Clayton [a,1], Hesam Jafarian [a,1], Ahmad Arabi Shamsabadi [d], Anupma Thakur [b,c], Rilyn Todd [a], Srinivasa Kartik Nemani [b,c,f], Mohtada Sadrzadeh [e], Mark Elliott [a], Babak Anasori [b,c,f,**], Leigh Terry [a,*]

[a] Department of Civil, Environmental, and Construction Engineering, University of Alabama, Tuscaloosa, AL 35487, USA
[b] School of Materials Engineering, Purdue University, West Lafayette, IN 47907, USA
[c] Department of Mechanical and Energy Engineering, Purdue School of Engineering and Technology and Integrated Nanosystems Development Institute (INDI), Indiana University-Purdue University Indianapolis, Indianapolis, IN 46202, USA
[d] Department of Chemistry, University of Pennsylvania, Philadelphia, PA 19104, USA
[e] Department of Mechanical Engineering, 10-367 Donadeo Innovation Center for Engineering, Advanced Water Research Lab (AWRL), University of Alberta, Edmonton, AB T6G 1H9, Canada
[f] School of Mechanical Engineering, Purdue University, West Lafayette, IN 47907, USA

HIGHLIGHTS

- $Ti_3C_2T_x$ MXene enhances performance in biofiltration-membrane hybrid systems.
- First exploration of MXene use in biofiltration-membrane hybrids for water treatment
- MXene integration boosts filtration efficiency and system stability.
- MXenes reduce fouling and increase durability in biofiltration-membrane hybrids.

GRAPHICAL ABSTRACT

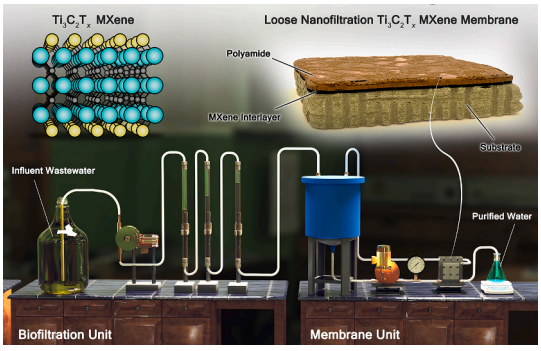

ARTICLE INFO

Keywords:
Biofiltration
MXenes, membrane modification
Loose nanofiltration
Water reuse

ABSTRACT

As the demand for sustainable and efficient water treatment solutions grows, the integration of advanced nanomaterials has become a focal point in enhancing membrane technologies. The purpose of this review is to provide a comprehensive and critical analysis of the current state of research on $Ti_3C_2T_x$ MXenes, highlighting their unique properties, the challenges they address, and the potential they hold for MXene-enhanced biofiltration-membrane systems. The perspective systematically examines how $Ti_3C_2T_x$ MXenes, with their exceptional electrical conductivity, hydrophilicity, and tunable surface chemistry, can be integrated into biofiltration-

* Corresponding authors at: Department of Civil, Environmental, and Construction Engineering, University of Alabama, Tuscaloosa, AL 35487, USA.
** Correspondence to: B. Anasori, Department of Mechanical and Energy Engineering, Purdue School of Engineering and Technology and Integrated Nanosystems Development Institute (INDI), Indiana University-Purdue University Indianapolis, Indianapolis, IN 46202, USA.
E-mail addresses: mdfirouzjaei@ua.edu (M. Dadashi Firouzjaei), banasori@purdue.edu (B. Anasori), leigh.terry@ua.edu (L. Terry).
[1] Jonathan Clayton and Hesam Jafarian Contributed equally to this work.

https://doi.org/10.1016/j.desal.2024.118198
Received 16 July 2024; Received in revised form 10 October 2024; Accepted 12 October 2024
Available online 15 October 2024

membrane systems to improve key performance metrics such as water flux, contaminant rejection, and fouling resistance. Various processes, including biofiltration, adsorption, and nanofiltration, are discussed, where $Ti_3C_2T_x$ MXenes have been shown to have a potential application. In addition to synthesizing existing literature, experimental validations are presented that demonstrate how MXene incorporation can alter membrane morphology and structure, leading to improved antibacterial properties and enhanced overall performance. These findings underscore the transformative potential of $Ti_3C_2T_x$ MXenes in developing next-generation biofiltration-membrane technologies that are not only more efficient but also more sustainable. Through this perspective, the key challenges that remain, such as cost implications and long-term stability, are identified, and future research directions are proposed to address these issues. This in-depth analysis highlights the critical role MXenes can play in advancing water treatment technologies, particularly in the context of water reuse, and encourages further interdisciplinary research in this rapidly evolving field.

1. Introduction

Membrane fouling remains a significant challenge, where particles and microorganisms in the feed solution accumulate on the membrane surface and block the pores [1]. This issue adversely impacts membrane performance, diminishing water flux and quality while shortening membrane lifespan, and increases operational costs [2]. Therefore, extensive efforts have been made to mitigate fouling before operation (enhancing membrane properties and feedwater pretreatment), during operation (optimizing operating conditions), and after operation (membrane cleaning). These strategies are broadly classified as physical and chemical methods [3].

Physical methods include optimizing operational parameters like crossflow velocity, pressure, and temperature. Backwashing and air sparging are also standard physical techniques for removing foulants from the membrane surface [4]. In contrast, chemical methods utilize cleaning agents such as acids, bases, or surfactants to dissolve and eliminate foulants. However, frequent chemical cleaning can damage membrane integrity and performance over time [5,6]. Both cleaning methods increase the operating cost and reduce the efficiency of membrane systems [3,7].

Another strategy to reduce fouling is membrane modification, which aims to alter membrane surface properties like topology and surface energy to enhance resistance to fouling [8,9]. Modification of membranes with hydrophilic materials [poly (ethylene glycol) (PEG), polyvinyl pyrrolidone (PVP), graphene oxide (GO), silica nanoparticles, silver nanoparticles (AgNPs), and zwitterions (zwitterionic sulfobetaine methacrylate (SBMA) [10–14]], can enhance water affinity, thereby reducing organic fouling [15]. Feed pretreatment methods such as coagulation, flocculation, and biofiltration are increasingly integrated into membrane systems to eliminate potential foulants before reaching the membrane [16]. These approaches to fouling mitigation are often combined to create strategies tailored to the specific requirements of each membrane application. Given their promising impact on improving membrane system efficiency, further exploration of fouling mitigation methods remains a crucial area of research.

Biofiltration is an efficient pre-treatment for membrane systems which reduces fouling and enhances the overall efficiency and longevity [17]. Biofiltration with different media such as sand or anthracite, supports microbial communities that biodegrade contaminants, minimizing their accumulation on the membrane surface. This strategy maintains consistent permeate flux, decreases the frequency of membrane cleaning, extends membrane lifespan, and lowers energy consumption and operational costs. Incorporating biofiltration enhances membrane-based water treatment's sustainability and economic viability [11]. Biofiltration is especially effective at removing biodegradable organic compounds and can potentially reduce chlorine demand in water treatment systems [18]. The removal of organic matter helps minimize byproduct formation, thereby contributing to the control of membrane fouling [19,20]. The efficiency of biofiltration is influenced by factors such as the type of filter media, flow rate, temperature, and the nature of the microbial community [21]. Optimization strategies for improving biofilter performance include adjusting empty bed contact times, temperatures, media size, backwashing schedules, and flow direction [22–24].

Biofiltration holds significant potential for potable water reuse, yet it faces limitations such as variable efficiency, limited removal of specific contaminants, and biofouling [25,26]. The choice of filter media, such as granular activated carbon (GAC), quartz sand, and anthracite, affects water quality [27–29]. The anthracite surface, which predominantly contains hydrophobic groups (C—C and C—H), is effective at adsorbing organic compounds from water sources [30,31]. Despite anthracite's effectiveness, drawbacks such as higher costs and biomass accumulation require further investigation [28,32,33]. GAC, a common biofilter medium, transforms into adsorptive to biological activated carbon (BAC) upon microbial colonization [34,35]. The transition time from adsorptive filters, such as GAC filters, to biofilters and the associated decrease in total organic carbon (TOC) removal during microbial growth, are notable concerns. Peterson and Summers found biofilters remove 70 % of TOC before 10,000-bed volumes but only 18 % after surpassing 40,000-bed volumes [25]. This decrease in TOC removal suggests that the adsorptive capacity of GAC filters exceeds the biodegradation capacities of biofilters. Despite these concerns, biofilters remain viable, particularly in potable reuse scenarios, as the total matter post-ozonation consists of 50–80 % biodegradable organic matter. Nonetheless, meeting potable reuse TOC limits (0.5–3 mg/L) will almost certainly necessitate additional treatment [25,36–38].

Biofiltration-membrane hybrid systems synergize the biological capabilities of biofiltration with the precise separation properties of membrane technology, enhancing water reuse treatment [39]. As a pretreatment stage, biofiltration employs microbial communities to degrade diverse contaminants, and the subsequent membrane stage, which selectively removes residual pollutants, pathogens, and fine particulates. This integrated approach enhances treatment efficiency, targeting a broader range of pollutants, including emerging contaminants and microorganisms, while meeting potable reuse TOC limits (0.5–3.0 mg/L) [39,40]. However, the microbial aspect introduces the risk of biofouling, where microorganisms accumulate on the membrane surface, compromising performance and water quality [41,42]. To counter this, antibacterial membranes are crucial in inhibiting bacterial growth, reducing biofilm formation, and ensuring sustained performance and treated water quality.

MXenes are a large family of two-dimensional (2D) transition metal carbides, nitrides, or carbonitrides [43]. The discovery of titanium carbide ($Ti_3C_2T_x$) MXene at Drexel University in 2011 marked the advent of this family of 2D materials [44]. The synthesis of $Ti_3C_2T_x$ MXene through top-down selective etching from a ternary titanium aluminum carbide (Ti_3AlC_2), which belongs to the family of ternary and quaternary transitional metal carbides called MAX phases, paved the way for exploring various 2D compositions [45]. MXenes have the chemical formula $M_{n+1}X_nT_x$, where M refers to early transition metal from groups 3 to 6, X denotes carbon and/or nitrogen, and T_x stands for surface terminations and functional moieties such as chalcogenides, halides, hydroxyl, imido, and amine groups. The variable '*n*' in the formula indicates the number of M-X-M layers, which can range from 1 to 4, and x in T_x is ≤ 2 [46,47]. Various synthesis methods have been

Table 1
Various etching processes for synthesizing MXenes.

Methods	MXene type	Etchants	Surface groups	References
Hydrofluoric acid (HF) etching	$M_3C_2T_x$ (M = Ti, V, Nb, Ta, MO, Hf, Zr)	50 wt% HF	—OH, —O, —F	[49]
	$Ti_3C_2T_x$	30 wt% HF/35 wt% H_2O_2	—OH, —O, —F	
		30 wt% HF/10 mL 1.85 M $(NH_4)_2S_2O_8$	—OH, —O, —F	
		40 mL 30 wt% HF/10 mL 1.25 M $FeCl_3$		
		37.5 mL 20 wt% HF/2.5 mL HNO_3		
Alkali etching	$Ti_3C_2T_x$	1 M NaOH + 1 M H_2SO_4	—OH, —O	[50]
		27.5 M NaOH		
		125 M KOH		
In situ HF formation etching	Ti_2CT_x	6 m LiF + 0.9 M HCl	—OH, —O, —F	[51]
	$Ti_3C_2T_x$	4 m NaF + 12 M HCl		
		4 M NH_4F + 12 M HCl		
		2 g FeF_3 + 6 M HCl	—OH, —O, —F	
		1 M $NaHF_2$		
		1 M KHF_2		
		2 M NH_4HF_2	—O, —F	
		12 m LiF + 9 M HCl		
		Ionic liquid ($EMIMBF_4$1-ethyl-3-methylimidazolium tetrafluoroborate/ $BMIMPF_6$ 1-butyl-3-methylimidazolium hexafluorophosphate)		
Electrochemical etching	$Ti_3C_2T_x$ M_3CT_x (M = Ti, V, Cr)	1 M NH_4Cl + 0.2 M TMAOH (tetramethylammonium hydroxide) 1 M HCl	—OH, —O, —Cl	[52]
Molten salt etching	$Ti_3C_2T_x$	ACl_2 (A = Zn, Cu, Cd, Fe, Co, Ni, Ag, & Cd)	—O, —Cl	[53]
		KF + LiF + NaF	—O, —F	
Other etching methods	M_3CT_x (M = Ti, MO)	I_2	—O, —OH, —I	[54]
		Ultraviolet light	—O	
		Surface acoustic waves (SWAS), LiF	—O, —OH, —F	
		Thermal reduction	—O, —OH	
		Algae	—O, —OH	

(Reproduced with permission from Elsevier [48].)

designed to produce MXenes with diverse structures and excellent physicochemical properties. Table 1 outlines various etching techniques used for synthesizing MXenes. Additionally, Fig. 1 represents the various MXene structures and possible elemental compositions.

MXenes have experienced rapid growth in applications, particularly in biomedical applications, electromagnetic interference shielding, environmental remediation, wastewater, and water reuse treatment [55–57]. Extensive research on 2D $Ti_3C_2T_x$ MXene has demonstrated its efficacy in identifying heavy metals such as lead (Pb), mercury (Hg), and cadmium (Cd), as well as detecting biomolecules and pathogens such as *Mycobacterium tuberculosis* in drinking water [58–60]. MXenes' high electrical conductivity (~21,000 S/cm for $Ti_3C_2T_x$) [61], tunable surface chemistry, and ease of solution processing (−40 to −60 mV zeta potential in aqueous media) [62] make them promising materials for biofiltration-membrane hybrid systems [63–65]. Additionally, MXene's antibacterial properties offer the potential to prevent biofouling, thereby extending the membrane's lifespan and maintaining efficiency [41,66]. Their high adsorptive capacity (4806 $mg.g^{-1}$ for Hg(II) removal) [67] improves TOC removal, which is crucial in water reuse scenarios requiring high levels of TOC reduction [25,55].

In addition to its antibacterial and adsorptive properties, the $Ti_3C_2T_x$ MXene has structural rigidity due to its high stiffness (~330 GPa for a single flake) [68,69]. Its stiff yet flexible 2D structure can be integrated into the membrane matrix to improve structural integrity, making the membrane more resistant to deterioration during backwashing operations [70,71] especially useful in varying flow rates and operational conditions.

This review aims to provide a comprehensive and detailed examination of the role of $Ti_3C_2T_x$ MXenes in enhancing biofiltration-membrane systems for water reuse applications. The study systematically covers the unique physicochemical properties of $Ti_3C_2T_x$ MXenes—such as electrical conductivity, hydrophilicity, and tunable surface chemistry—that make them suitable for integration into membrane technologies. The review discusses how these properties can be leveraged to improve critical performance metrics of biofiltration-membrane systems, including water flux, contaminant rejection, and fouling resistance. Furthermore, the article presents both a synthesis of existing literature and experimental validation on how MXenes can alter membrane morphology and antibacterial properties. Key challenges, such as cost implications, long-term stability, and scalability, are identified, and future research directions are proposed. This review, therefore, provides a thorough analysis of the current advancements in MXene-enhanced biofiltration and offers insight into the future development of next-generation water treatment systems.

2. Insights into MXene's applications in biofiltration-membrane hybrid treatment

2.1. Potentials and challenges of using MXenes in biofilter media

The addition of antimicrobial materials in biofilter membranes offers significant benefits in combating harmful bacteria. However, it is crucial to mitigate the potential risks to useful microorganisms. To balance these advantages and risks, selective targeting using antibacterial nanomaterials with tunable properties such as MXenes can be achieved. MXenes with tunable compositions, atomistic structure, and surface chemistry can mitigate these risks and harness their full potential in a responsible and sustainable manner in biofiltration treatment [39]. For example, the surface chemistry of MXenes can be engineered to target specific harmful pathogens selectively with minimal impacts on beneficial bacteria [72]. This would necessitate precise control and understanding of MXene chemical and physical interactions with various microbial species [73]. Direct physical contact between the sharp edges of MXene sheets and a microbe's membrane can rupture the membrane, leading to microbial death [74]. Light absorption by MXenes can further enhance their biocidal activity, causing simultaneous chemical inactivation of microbes through the reactive oxygen species (ROS) and heat generation [73]. Additionally, the oxidation of MXenes releases small amounts of metal ions, aiding in microorganism deactivation.

Although MXenes offer exciting potential for enhancing the antibacterial properties of biofilter membranes, there are several challenges that need to be addressed. MXenes' antimicrobial features find value in applications prioritizing the removal of biological contaminants, such as viruses or pathogens, rather than their biological transformation [75]. Another issue is the possibility of leaching metal ions from MXenes into treated water. Because MXenes are transition metal carbides or nitrides, they may introduce metal ions into water, raising concerns about the material's long-term stability and the potential for toxicological effects. This is especially critical in applications targeting potable water production, where adherence to strict water quality regulations is paramount. Metal ion leaching may require additional treatment steps, complicating water treatment processes and increasing operational costs. [73]. Generating robust data to support regulatory environmental approval and establishing standards for the safe use of MXene-based biofilter media is critical. Finally, MXenes tend to aggregate in the structure of biofilter membranes during fabrication steps, which can

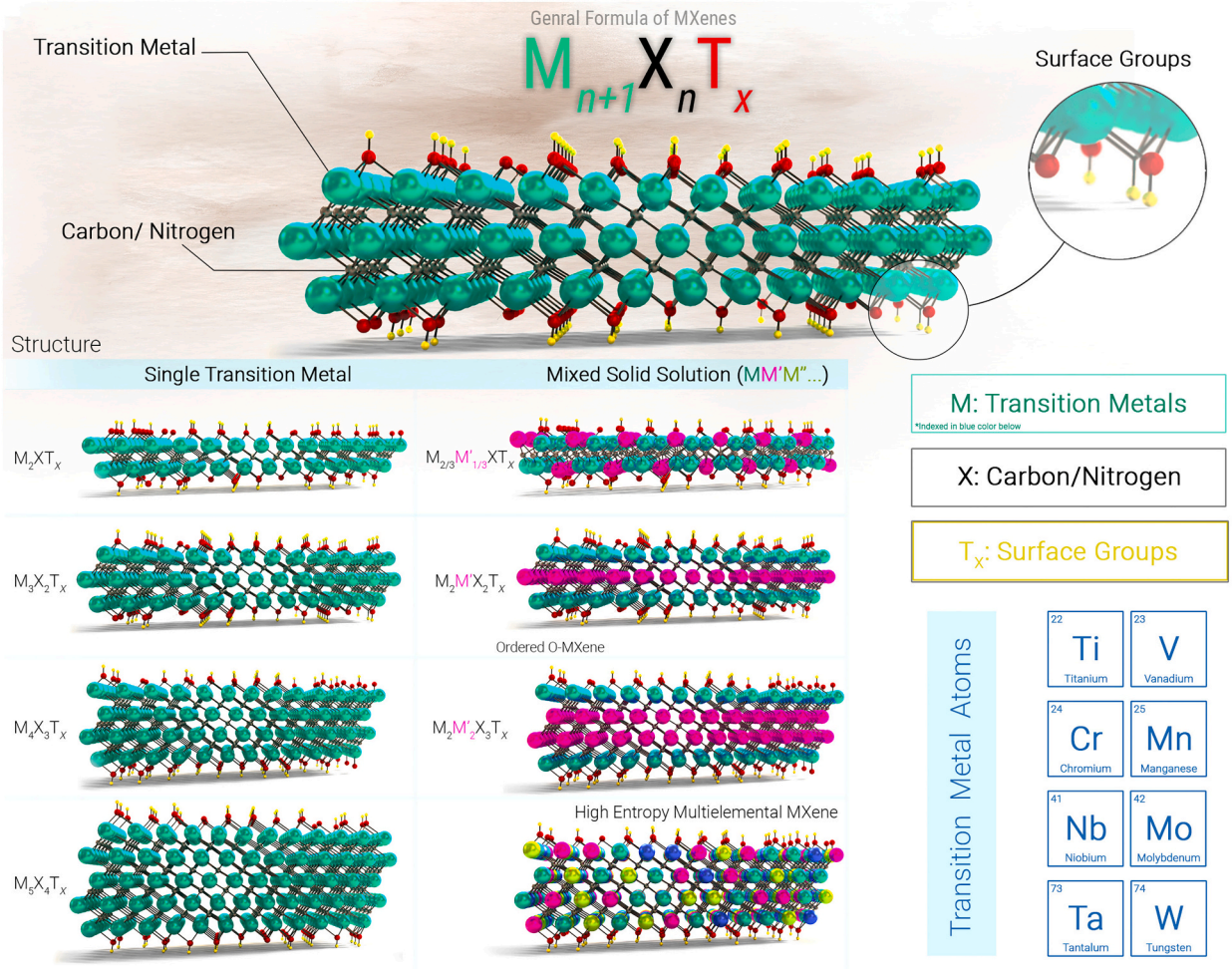

Fig. 1. Schematic of MXenes with various structures and potential building blocks. The most commonly studied MXene is $Ti_3C_2T_x$, but a variety of MXenes with different M elements have been synthesized, including titanium (Ti), vanadium (V), niobium (Nb), molybdenum (Mo), and tantalum (Ta). Variations in the X element, typically carbon (C) or nitrogen (N), and different surface termination combinations, further broaden the MXene family. These structural variations significantly impact MXenes' electronic, mechanical, and chemical properties, making them versatile materials for various applications [55].

decrease their effective surface area and compromise their antibacterial efficacy. Developing methods to help well dispersion of MXenes into biofilter membrane networks can address this issue.

2.2. MXene as a post-treatment adsorbent

MXenes have a high potential for use as post-treatment adsorbents in biofiltration systems due to their large surface area and tunable surface chemistry. These attributes make them particularly effective in addressing residual contaminants that may persist after primary biological filtration treatment. MXenes can be tailored for selective adsorption of various pollutants, including residual organic compounds, heavy metals, and specific pathogens, thereby enhancing the overall efficiency of the biofiltration process [76]. The adsorption mechanisms rely on electrostatic interactions and ion exchange, with their effectiveness influenced by water quality parameters such as pH, temperature, and the presence of background ions and natural organic matter (NOM) [76,77].

Regarding water quality, the adsorption performance of MXenes improves with increasing pH levels [76]. Acidic conditions limit the material's negative surface charge, reducing adsorption capacity due to competition between hydrogen ions and positively charged target compounds. As pH increases, MXene's surface charges become more negative, consequently increasing its adsorption capacity [78–80]. Temperature is another critical factor affecting MXenes' adsorption capability. High temperatures (up to 55 °C) make the adsorption process endothermic and spontaneous, thereby increasing adsorption feasibility through alterations in thermodynamic parameters [79]. In the presence of background ions and NOM, MXene-based adsorbents exhibit selective adsorption of target molecules, displaying a preference for divalent and multivalent ions over monovalent ions. Importantly, MXene-based adsorbents demonstrate good recyclability, maintaining high adsorbate removal rates of 80–90 % after multiple regeneration cycles, contributing to their sustainability and cost-effectiveness [81,82]. Table 2 summarizes the adsorptive removal of selected inorganic and organic contaminants by MXenes and their hybrid nanomaterials, as well as the study's main findings [76].

While the potential of MXenes appears promising, practical implementation still presents challenges such as long-term stability, potential toxicity, uniform distribution, reusability, and manufacturability that will necessitate additional research and development. Computational studies and molecular modeling can help to optimize MXenes' atomistic design for specific adsorption processes. However, uncertainties about MXenes' long-term stability under various environmental conditions and concerns about their potential toxicity necessitate generating robust data through research studies. Furthermore, scaling up the synthesis of tailored MXenes for industrial applications while preserving their specific adsorption properties requires conducting pilot studies.

Table 2
Summary of MXenes and MXene-based nanocomposites' adsorption efficacy for the removal of selected inorganic and organic contaminants.

MXene	Species	q_m (mg g^{-1})	C_0 (mg/L)	T (K)	pH	Main finding	Ref.
$Ti_3C_2T_x$ $Ti_3C_2T_x$-DMSO-hydrated	Uranium (IV)	214 5–220	100 298	293	5	Enhanced adsorption on hydrated $Ti_3C_2T_x$ compared to dry $Ti_3C_2T_x$ due to its flexibility and large interlayer spacing. High adsorbed efficacy of hydrated and intercalated MXene towards dye chemicals and heavy metal ions.	[83]
DL-$Ti_3C_2T_x$	Copper	78.5	10–350	298–318	2–5.5	~Threefold higher adsorption capacity of $Ti_3C_2T_x$ than commercial activated carbon. Excellent Cu adsorption due to large surface area, functional groups, and dispersibility of the adsorbents (reached equilibrium in 3 min).	[84]
$Ti_3C_2T_x$	Barium	9.3	1–55	298	3.9	Higher adsorption than other adsorbents: Maximum adsorption capacity of 9.3 mg g^{-1}	[85]
$Ti_3C_2T_x$ Alk-$Ti_3C_2T_x$	Barium (II)	12 46.5	50–500	RT	1–10	High adsorption capacity on Alk-$Ti_3C_2T_x$ (46 mg g^{-1}), approximately three times greater than unmodified $Ti_3C_2T_x$.	[86]
$Ti_3C_2(OH)_{0.8}F_{1.2}$	Chromium	62	10	298–333	1–7	MXene that has been chemically exfoliated in solutions containing F ions has a surface covered with F groups.	[87]
Sodium alginate/ $Ti_3C_2T_x$	Copper Lead	87.6 383	0–10 mM	298–333	1–7	Achieved high adsorption capacity of selected inorganic compounds on the MXene/alginate composite and reached equilibrium in 15 min due to its abundant adsorption sites.	[88]
Ti_2CT_x-hydrated	Thorium (IV)	213	5–180	282–312	1–3.5	Enhanced adsorption due to the inner-sphere complexation caused by the strong attraction between Ti-OH and Th (IV).	[89]
$Ti_3C_2T_x$	Cesium (I)	25.4	5–300	273–303	2–12	Reached the maximum adsorption capacity on $Ti_3C_2T_x$ in 1 min at room temperature.	[90]
Magnetic $Ti_3C_2T_x$	Mercury (II)	1128	25–1000	288–318	2–9	The higher adsorption capacity of magnetic $Ti_3C_2T_x$ compared to other two-dimensional materials.	[91]
K-HTNs Na-HTNs	Europium (III)	203 222	20–300	298	2–10	Improved adsorption of Eu (III) upon exchange with cations in the active sites of MXene due to electrostatic interaction and H bonding.	[92]
$Ti_3C_2T_x$-10 %	Chromium (VI)	250	208	RT	2–13	Effectively reduced Cr (VI) to less toxic Cr (III) species, making residual Cr (VI) in treated water far below the World Health Organization's drinking water standard.	[93]
Alk-Ti_2C sheet	Cadmium	326	19.6–562	RT	2–9	Successful adsorption of heavy metals and other contaminants on the fluoride-free exfoliated Ti_2AlC MAX phase.	[94]
e-TACSs e-TACFs	Lead (II)	218 284	200	298–328	2–11	The significantly high adsorption capacity of the e-TACFs and e-TACSs was prepared using a hydrothermal and fluoride-free method.	[95]
Mxene-25 Mxene-35 Mxene-45	Lead	119 164 185	100	293–313	0–5	Significant impact of exfoliation temperature had on the interlayer structure and morphology of MXene (higher exfoliation temperatures yield larger d-spacing and surface area).	[96]
$Ti_3C_2T_x$	Chromium	80	100	298	–	Decent capacity but slow adsorption of $Ti_3C_2T_x$ (80 mg g^{-1} in 8 h).	[97]
MX-SA2:20 MX-SA4:20	Mercury	365 933	25–994	298	0–11	Excellent adsorption capability of MX-SA4:20 even under highly acidic conditions (pH 0).	[98]
MTC-P TCNS-P	Rhenium (VII)	42.1 363	5–400	–	1–10	High adsorption upon modification of Ti_2CT_x nanosheets	[99]
Ti_2CT_x	Uranium (VI)	470	5–400	–	1–10	Very high but slow adsorption, (reached equilibrium within 48 h, and the adsorption capacity of 470 mg g^{-1} at pH 3).	[100]
V_2CT_x	Uranium (VI)	174 (qe)	5–120	RT	3–5	Ion exchange as the dominant adsorption mechanism on multilayered V_2CT_x (reached equilibrium after 4.5 h and a maximum adsorption capacity (174 mg g^{-1} at pH 5).	[101]
$Ti_3C_2T_x$	Methylene blue	140	5–40	293–313	3.9–9.5	Reached equilibrium quickly (within 30 min) due to the electrostatic interaction between MXene and methylene blue.	[102]
$Ti_3C_2T_x$	Urea	21.7	30–450 mg/dL	RT-313	–	High selective urea adsorption on MXene (94 %), with no significant impact on cell viability or hemocompatibility.	[103]
MXene@Fe_3O_4	Methylene blue	11.7	1–40	298–328	3–11	The key mechanism in pH above 5.1: electrostatic force caused by the adsorbent's pH and affinity to Ti site and OH groups.	[79]

C_0 = initial concentration; q_m = maximum adsorption capacity; temp. = temperature; SA = sodium alginate; TACSs = Ti_3AlC_2 nanosheets; TACFs = Ti_3AlC_2 nanofibers; DMSO ¼ dimethyl sulfoxide; HTNs = hierarchical titanate nanostructures; PEI = polyethyleneimine; PAA = poly acrylic acid; PDDA = poly (diallyldimethylammonium chloride); MTC-P = multilayer Ti_2CT_x/PDDA composite; TCNS-P = Ti_2CT_x nanosheet/PDDA composite; DL = delaminated.

2.3. The synergy of loose nanofiltration post-biofiltration

2.3.1. Optimized loose nanofiltration membranes

Loose nanofiltration (LNF), which operates at lower pressures (3–5) bar and utilizes membranes with pore sizes ranging from 1 to 5 nm, is emerging as a versatile and cost-effective water treatment technology, particularly effective for post-biofiltration treatment [76,104,105]. Renowned for high selectivity and energy efficiency, LNF membranes are ideal for drinking water treatment [106,107]. Compared to tighter nanofiltration and reverse osmosis membranes, LNF membranes generally offer higher permeate flux, enhancing the efficiency and speed of separation processes [108]. LNF excels at removing larger dissolved solutes and organic molecules while preserving beneficial monovalent ions [109,110]. This process provides a targeted and efficient solution when combined with biofiltration. Biofiltration removes organic matter and specific contaminants, while LNF refines the effluent by capturing residual contaminants. The adaptability of LNF membranes, which can be customized for specific contaminants, makes them a promising component for advanced water reuse treatment, efficiently and comprehensively meeting stringent quality standards [104,108].

LNF membranes are typically manufactured using techniques such as phase inversion, interfacial polymerization, and electrospinning [111,112]. Among these techniques, interfacial polymerization stands out for fabricating thin-film composite (TFC) membranes, which are widely used in nanofiltration and reverse osmosis [113,114]. This method allows for precise control over pore size, thickness, and surface chemistry, which is essential for achieving the desired filtration characteristics in LNF membranes. By adjusting parameters such as monomer concentration, reaction time, and temperature, membrane properties can be finely tuned to meet specific requirements [111,115].

Table 3
Summary of MXene-based membranes performance for the organic and inorganic pollutants removal.

Membrane/support materials	Fabrication method	Thickness (μm)	Pore size/d-spacing (nm)	Pollutant	Water permeability (L m^{-2} h^{-1} bar^{-1})	Rejection (%)	Key experimental results	Ref.
$Ti_3C_2T_x$@Fe_3O_4/CA	Vacuum filtration	3.4	–	Ion	96.8	Cr^{+6}: 70.2 % Cd^{+2}: 64.1 % Cu^{+2}: 63.2 %	Retained 83.7 % flux and 76 % removal efficiency after 3 cycles, restored by HCl washing.	[124]
$Ti_3C_2T_x$@NH_2-MIL-101(Al)/PVDF	Non-induced phase separation + interfacial polymerization	–	1.4 (pore size)/0.84 (d-spacing)	Ion	17.1	>95.2 % for Ni^{+2}, Cd^{+2}, Mn^{+2}, Cu^{+2}, Zn^{+2} Mn^{+2}: 97.6 %	The intercalated structure increases d-spacing for better water transport. Enhanced rejection of salts and heavy metals due to the hydrophilic and negatively charged surface of MXene.	[125]
Hydroxylated $Ti_3C_2T_x$/PTFE	Vacuum filtration + thermal self-crosslinking	383	1.508 (d-spacing)	Ion	–	Heavy metal cations (Pb^{+2}, Cu^{+2}, Cd^{+2}): 99.5 % Anions (Cl^-, NO_3^-): ~97 %	Improved hydrophilicity due to the presence of the MXene increases wettability and ion transport. Suppresses swelling by thermal self-crosslinking, maintaining interlayer spacing.	[126]
$Ti_3C_2T_x$@carbon nanofibers (CNFs)/PVP	Electrospinning + carbonization	–	1.34 (d-spacing)	Ion	–	Pb^{+2}: 89 % As^{+2}: 81 %	Improved ion adsorption due to increased interlayer spacing and MXene's large specific surface area and abundant active sites. High removal rate for Pb^{2+} and As^{3+} at low concentrations (10 ppb to 10 ppm). High reusability for up to 4 cycles.	[127]
$Ti_3C_2T_x$/modified PPSU	Non-induced phase separation	–	0.8–1.6 (pore size)	Ion	11.1 (for 0.6 wt% MXene)	Pb^{+2}: 94 % Cu^{+}2: 97.4 % Cd^{+2}: 97.4 %	High antifouling performance with recoverable flux after backwashing due to MXene's surface properties.	[123]
$Ti_3C_2T_x$@poly-melamine-formaldehyde/nylon	Vacuum filtration + glutaraldehyde crosslinking	7	–	Ion/dye	381.2	Zn^{+2}: 96.2 % Pb^{+2}: 91.7 % CV: 96.4 %	Significant increase in water permeability (405 % of pure MXene membrane). High adsorption rates for heavy metals and organics (Zn^{2+}, Pb^{2+}, Phenol, CV) due to the synergy between MXene and PMF active sites.	[128]
$Ti_3C_2T_x$@TiO_2/alumina	Spin coating (disc) + dip coating (hollow fiber)	~2	6.6 (pore size)	Dye	>90 for hollow fiber membranes	90 %	Increased stability and pore control with 2D MXene acting as "floor tiles". Enhanced water flux and selectivity with MXene incorporation.	[129]
$Ti_3C_2T_x$@Al_2O_3/nylon	Vacuum filtration and self-assembly	–	d-Spacing: 1.49 nm (dry state) to 1.75 nm (wet state)	Dye	88.8	RB: 99.8 % MB: 99.5 %	Outstanding rejection rates for organic dyes (>99 %). Enhanced water permeability due to Al_2O_3 intercalation, preventing MXene layer compaction. Improved membrane stability through ionic crosslinking between Al_2O_3 and MXene.	[130]
$Ti_3C_2T_x$@CNTs@CTAB/PEI	Vacuum filtration	0.496–1.1	1.4–1.5 (d-spacing)	Dye	20.1–100.9	CR: >95 %	Significant increase in anti-pressure and anti-swelling properties. Pillaring with CNTs improved interlayer spacing, preventing compaction.	[131]
GO@$Ti_3C_2T_x$/nylon	Vacuum filtration	0.14	1.27 (d-spacing)	Dye	Water: 42 Acetone: 48.32, Methanol: 25.03, Ethanol: 10.76 IPA: 6.18	>90 %	Increased Interlayer Spacing by incorporating MXene, enhancing solvent permeation. Maintained stability in organic solvents for long-term operation.	[132]
GO@$Ti_3C_2T_x$/MCE	Vacuum filtration	0.55	–	Dye	71.9 L/m^2 h^{-1} bar^{-1}, 11 times more than the pure GO membrane (6.5 L/m^2 h^{-1} bar^{-1})	99.5 % for NR, MB, CV, BB 100 % for HA, BSA	MXene increased interlayer spacing and reduced oxygen-containing functional groups on GO, improving water flux and lowering water flow resistance. Near-complete removal of	[133]

(*continued on next page*)

Table 3 (*continued*)

Membrane/support materials	Fabrication method	Thickness (μm)	Pore size/d-spacing (nm)	Pollutant	Water permeability (L m^{-2} h^{-1} bar^{-1})	Rejection (%)	Key experimental results	Ref.
							Natural Organic Matter (HA and BSA).	
DGO@$Ti_3C_2T_x$/PVDF	Vacuum filtration	2	0.73 (d-spacing)	Dye/ion	63.5	DR28: 98.1 % Direct Black 38: 96.1 %	Demonstrated excellent mechanical stability and anti-swelling properties due to dopamine functionalization.	[134]
$Ti_3C_2T_x$/PVDF	Vacuum filtration	1.5	d-Spacing: 0.64 in wet state	Dye	37.4	MB ~100	Stable rejection of large dye molecules.	[135]

CA = cellulose acetate; PVDF = polyvinylidene fluoride; PTFE = polytetrafluoroethylene; PVP = polyvinylpyrrolidone; PPSU = polyphenylsulfone; CNT = carbon nanotubes; CTAB = hexadecyl trimethyl ammonium bromide; PEI = polyethyleneimine; GO; graphene oxide; MCE = mixed cellulose ester; DGO = dopamine-functionalized graphene oxide; CV = crystal violet; RB = rhodamine B; MB = methylene blue; CR = congo red; NR = neutral red; BB = brilliants blue; HA = humic acid; BSA = bovine serum albumin; DR28 = direct red 28.

Interfacial polymerization is highly adaptable, enabling the incorporation of functional groups or nanoparticles to enhance performance characteristics such as fouling resistance. The resulting thin-film composite membranes, featuring a dual-layer structure that combines mechanical strength with selectivity, are particularly advantageous for LNF applications requiring both attributes. This method is scalable, straightforward, and well-suited for industrial use [111,115]. LNF membranes, with a molecular weight cut-off (MWCO) of around 1000 Da and significant negative surface charges, are promising for drinking water treatment. Approximately 90 % of NOM falls within the molecular weight range of 500–3000 Da. Similar to traditional nanofiltration membranes, LNF membranes utilize steric exclusion and electrostatic effects to reject charged solutes [106,116].

As previously mentioned, various methods can be employed in fabricating LNF membranes via interfacial polymerization to achieve tailored properties. By adjusting monomer concentrations in both phases, the density and permeability of the membranes can be influenced. Higher concentrations typically result in denser, less permeable membranes [117]. However, surpassing the ideal monomer concentrations may detrimentally affect both water flux and rejection rates [118]. Hence, it's imperative to tailor the monomer concentration to suit each application. Another approach involves adjusting reaction time and temperature, where shorter durations and lower temperatures typically yield thinner films with larger pores, suitable for applications like LNF. Careful selection of monomers is also pivotal, encompassing aqueous phase options like piperazine or *m*-phenylenediamine and organic phase candidates like trimesoyl chloride. These monomers can be interchanged or supplemented with others to customize membrane properties. Additionally, incorporating additives like surfactants and nanomaterials into monomer solutions can alter membrane characteristics such as hydrophilicity, mechanical strength, and resistance to fouling [119,120]. Methods such as heat treatment or chemical cross-linking after fabrication provide further options for tuning membrane properties. The adaptability of the interfacial polymerization technique enables the precise customization of LNF membranes to meet specific requirements of various applications, rendering it a highly efficient fabrication method [117,118].

2.3.2. *MXene-enhanced loose nanofiltration membranes*

Incorporating MXenes into networks of LNF membranes can improve membrane properties in several ways. The notable mechanical robustness of MXenes significantly enhances the membrane's durability, a crucial factor for LNF membranes operating under varying pressures [119]. Moreover, MXenes have a large surface area and various tunable surface functional groups, enhancing filtration efficiency by interacting with contaminants and improving membrane selectivity. To increase salt rejection rates of polyamide nanofiltration membranes, Xui and Zhang incorporated MXene flakes into the organic phase during interfacial polymerization and compared the efficacy of the fabricated membrane with those of membranes with MXene embedded in the aqueous phase as well as the unmodified membrane [121]. This strategy resulted in a nanocomposite nanofiltration membrane with enhanced surface charge but reduced effective pore size. During a 28-day continuous permeation test, the MXene membrane achieved a Na_2SO_4 rejection rate of 98.6 %, outperforming membranes with MXene embedded in the aqueous phase as well as the unmodified membrane. Long-term water immersion tests demonstrated that the MXene membrane maintained high salt rejection even after being submerged in water for up to 105 days, indicating the stability of MXene on the membrane surface despite significant surface coverage.

The chemical versatility of MXenes allows for the customization of membrane properties such as pore size, topology, and hydrophilicity which are particularly important for achieving high permeability and low fouling in LNF membranes [122]. Finally, the high conductivity of MXenes proves advantageous in applications requiring electrochemical activation or fouling mitigation through electrochemical methods [119,122]. A previous study reports the efficacy of nanocomposite NF membranes composed of polyphenylsulfone (PPSU) polymer MXene nanosheets for removing heavy metals from wastewater [123]. The nanocomposite membranes showed a substantial improvement in surface roughness, achieving approximately a 50 % smoother surface compared to the control PPSU membrane. Additionally, the wettability of the nanocomposite membrane improved progressively, reaching a maximum of 0.6 wt% MXene ratio (contact angle = 49.4°), compared to 60.3° for the control membrane. The mean pore size increased from 0.84 nm in the control membrane to 1.6 nm in the 0.6 wt% MXene-modified membrane, though the porosity remained consistent across all membranes at around 79 %. Performance evaluations revealed that incorporating MXene led to a 28 % increase in pure water flux, recording 3.8 LMH with only 0.1 wt% MXene. The highest flux (11.1 LMH) was observed in the nanocomposite membrane with 0.6 wt% MXene, compared to 2.74 LMH for the control PPSU membrane. The retention rates of metal ions were similar across all membranes. The nanocomposite membranes also demonstrated excellent antifouling properties, which correlated with the MXene content. Even with a 20 % reduction in fouling for the 0.1 wt% MXene-modified membrane, the flux was largely recoverable and remained significantly higher than that of the control PPSU membrane. Although a direct comparison of various MXene-based membranes is impractical because membrane performance is best evaluated under similar conditions, the goal is to investigate the efficiency of MXene nanocomposite membranes for the organic and inorganic pollutants removal from wastewater. So, a comparative analysis of the performance of MXene nanocomposite membranes prepared using various design strategies for the removal of selected pollutants is presented in Table 3.

Capitalizing on the compelling advantages offered by MXenes, we fabricated novel LNF polyamide membranes incorporated by $Ti_3C_2T_x$ MXene nanosheets. To rigorously assess the efficacy of MXene-based

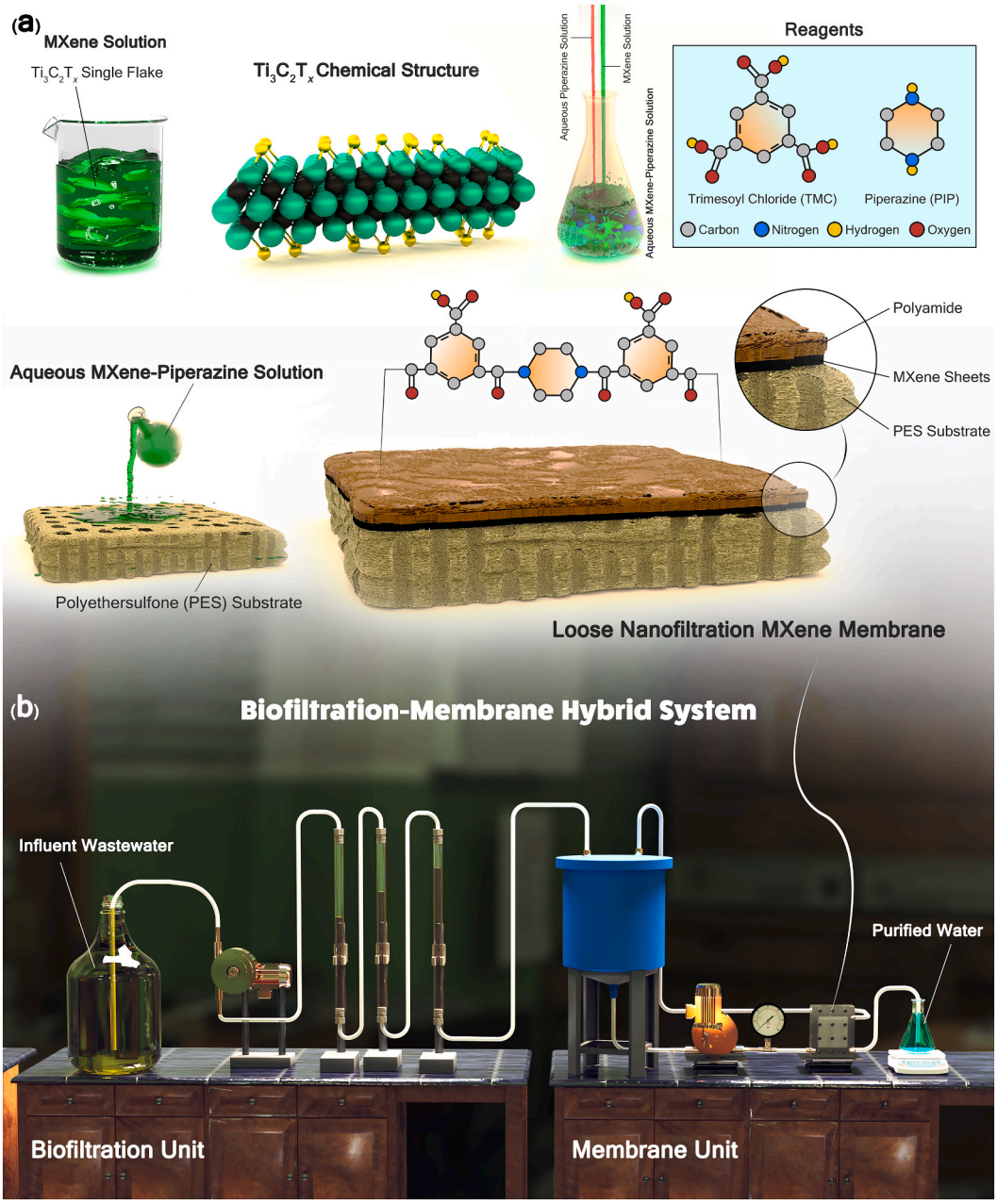

Fig. 2. The $Ti_3C_2T_x$ MXene structure and its strategic integration into the LNF MXenes membrane which is then incorporated into a hybrid biofiltration-membrane water treatment system. (a) The schematic illustration of $Ti_3C_2T_x$ MXene, and loose nanofiltration (LNF) $Ti_3C_2T_x$ MXene polyamide membrane. (b) The schematic illustration of a combined biofiltration-membrane hybrid unit. This diagram depicts the novel membrane's design, emphasizing the targeted incorporation of MXenes to improve properties like antibacterial activity, adsorptive capacity, and mechanical reinforcement.

membranes, we conducted a comparative analysis and evaluated their performance metrics against those of conventional NF polyamide membranes (Materials and method section regarding these experiments were discussed in the Supplementary information). This comparative study aims to elucidate operational efficiencies, including contaminant removal rates and water fluxes, offering valuable insights into the potential benefits of incorporating MXenes into biofiltration-membrane hybrid systems for water reuse systems. Additionally, Fig. 2 provides the schematic illustration of the $Ti_3C_2T_x$ MXene structure, its integration with the LNF membranes, and its incorporation into hybrid biofiltration-membrane water treatment systems.

Fig. 3 depicts a detailed analysis of the structural and morphological properties of both unmodified and MXene-incorporated LNF membranes. The X-ray diffraction (XRD) patterns of Ti_3AlC_2 MAX and $Ti_3C_2T_x$ MXene (Fig. 3a) confirm that the MAX phase was successfully converted to MXene. Scanning electron microscopy (SEM) images of MXene sheets on an aluminum oxide support (Fig. 3b_1) show single flakes of $Ti_3C_2T_x$ MXene, indicating effective MXene delamination (Fig. 3c–e). SEM images of the pristine porous polyethersulfone (PES) substrate display a uniform surface with visible pores (Fig. 3c_{1-2}). In contrast, SEM images of the polyamide-loose nanofiltration (PA-LNF) membranes show a more textured surface, indicating the formation of the polyamide layer via interfacial polymerization (Fig. 3d_{1-2}).

The incorporation of MXene resulted in a noticeable change in the surface morphology of the polyamide membrane, as evident in the SEM images (Fig. 3e_{1-6}). Images of 0.04 wt%, 0.1 wt%, and 0.5 wt% MXene-LNF membranes reveal distinct surface morphology and texture variations, which become more pronounced as the MXene concentration

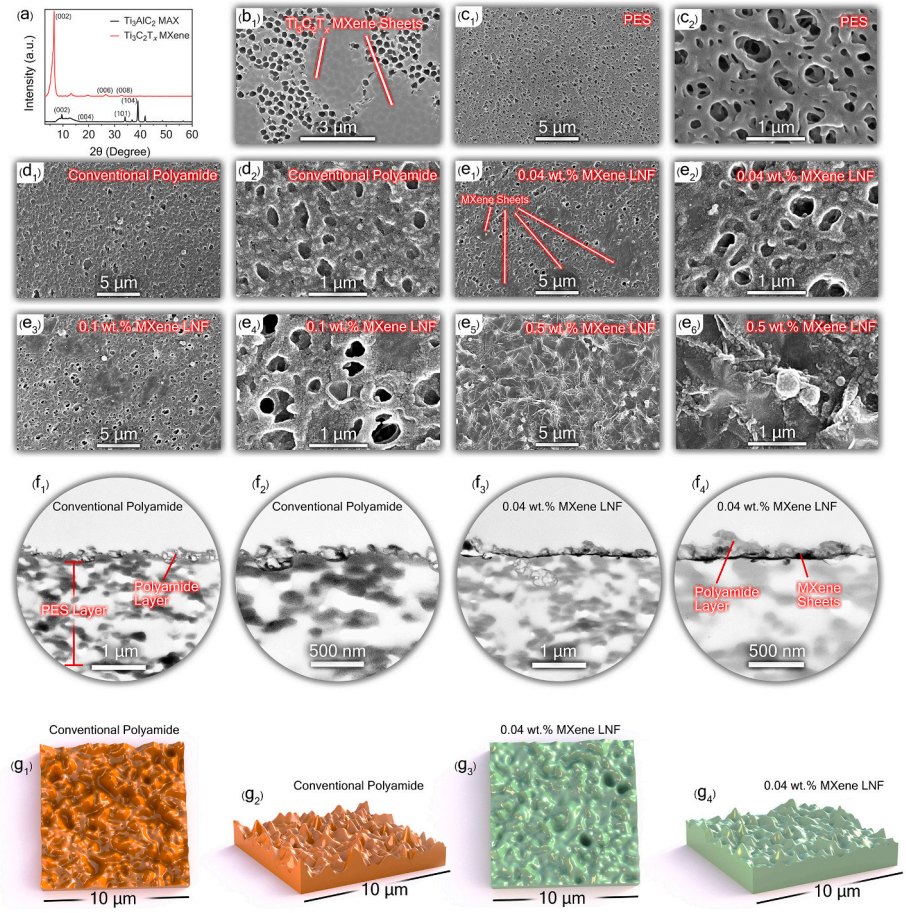

Fig. 3. A detailed structural and morphological analysis of unmodified and MXene-incorporated PA-LNF membranes. (a) The XRD patterns confirm the successful conversion of Ti_3AlC_2 MAX to $Ti_3C_2T_x$ MXene, and (b–e) the SEM images show the surface morphology and uniform dispersion of MXene within the polyamide matrix. (f) TEM images indicate a well-dispersed MXene interlayer between the polyamide and PES layers, which has implications for membrane performance and stability. Notably, the created interlayer positioning improves MXene's oxidation resistance, extending its functional lifespan within the membrane. (g) AFM measurements show that MXene incorporation slightly reduces surface roughness, with the 0.04 wt% MXene-LNF membrane exhibiting a lower R_a of 109.2 nm compared to 118.7 nm for the conventional PA-LNF membrane. MXene is a promising material for improving membrane performance in biofiltration-membrane hybrid systems due to its appealing feathers, which could reduce fouling and improve separation efficiency.

increases. This change in surface morphology suggests that MXene nanosheets integrate into the polyamide matrix, potentially influencing the membrane's pore structure and tortuosity. The well dispersion of MXene within the polyamide layer is crucial for achieving improved membrane properties. The varied surface textures at different MXene concentrations indicate that MXene's inclusion likely influences key transport properties such as the water flux and solute rejection, necessitating effective optimization for obtaining improved, repeatable, and reproducible outcomes [136].

Cross-sectional transmission electron microscopy (TEM) images provide insight into the interface between the constituent layers (Fig. 3$f_{1–4}$). The high aspect ratio and atomistic structure of MXene sheets can facilitate a uniform material distribution within the polyamide matrix [137]. The formation of an MXene layer in the interface of the polyamide and PES layers can be observed by comparing the TEM images of the 0.04 wt% MXene-LNF (Fig. 3$f_{3–4}$) and the unmodified PA-LNF membrane (Fig. 3$f_{1–2}$). Introducing the MXene layer can alter the transport properties of the modified membranes. The uniform dispersion of MXene within this interlayer is crucial for achieving consistent membrane performance. The coverage of the MXene interlayer by both PES and polyamide layers enhances MXene stability by preventing MXene flakes from being exposed to oxygen. In addition, embedding MXene sheets within the membrane network can protect them from direct exposure to the aqueous environment, enhancing their stability against hydrolysis and oxidation [138]. Preserving MXene's structural integrity is crucial for long-term applications where membrane longevity is paramount.

Incorporating MXene into the polyamide selective layer also slightly reduces membrane surface roughness, most likely due to less penetration of the aqueous monomer solution into the substrate during interfacial polymerization as measured by atomic force microscopy (AFM). The PA-LNF unmodified membrane had an average roughness (R_a) of 118.7 ± 5.1 nm, while the 0.04 wt% MXene-LNF membrane had a lower R_a of 109.2 ± 4.8 nm. A smoother surface is less prone to fouling due to reduced foulants adhesion sites, an essential consideration in membrane-based water treatment processes [139,140]. Furthermore, reduced roughness may result in more uniform flow distribution and enhanced flow dynamics across the membrane surface, improving overall transport and antifouling properties. Finally, a more straightforward membrane cleaning process can remove attached species on the surface due to less trapped foulants in the surface irregularities. Besides improved surface topology, MXene's inherent hydrophilicity can improve the polyamide surface's wetting properties, promoting more efficient water spreading and reducing the formation of water clusters or droplets. This is particularly crucial in membrane filtration processes, where surface wetting influences transport and antifouling properties [137,139].

The results discussed earlier show that MXene incorporation causes

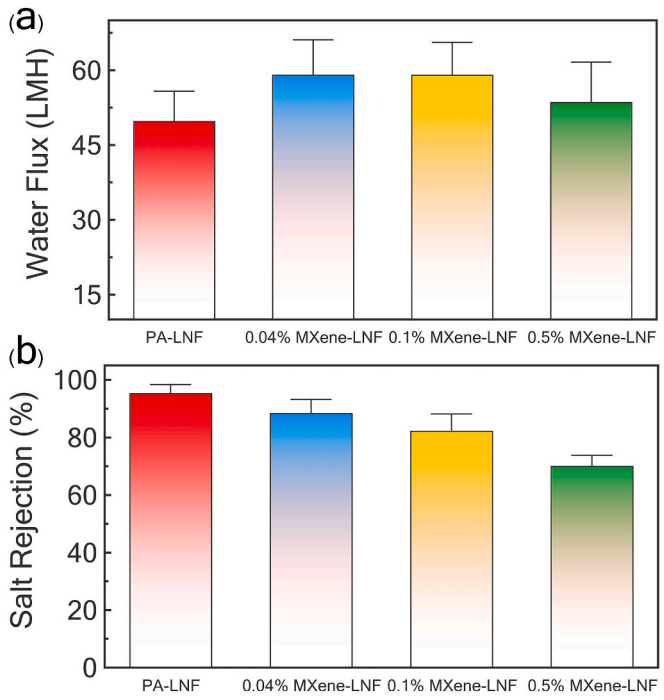

Fig. 4. (a) Water flux and (b) sodium sulfate rejection rate for PA-LNF and MXene-LNF membranes at various MXene concentrations were compared. According to the graph, the PA-LNF membrane has a water flux of 49.8 ± 6.0 LMH and a high sodium sulfate rejection rate of 95.4 ± 3.0 %. MXene-LNF membranes, on the other hand, show an increase in water flux at 0.04 wt% and 0.1 wt% MXene concentrations (59.1 ± 6.5 LMH), but a slight decrease at 0.5 wt% (53.6 ± 8.0 LMH). Concurrently, sodium sulfate rejection rates fall from 88.5 ± 4.8 % at 0.04 wt% MXene to 70.1 ± 3.7 % at 0.5 wt% MXene, indicating a trade-off between increased water flux and reduced salt rejection rate upon MXene incorporation.

significant changes in membrane morphology, structure, and topology. With the observed changes in the structural and physical properties of the membrane, we anticipate variations in water flux and contaminant rejection rates. To evaluate the influence of MXene incorporation into the PA-LNF on the membrane transport properties, the capability of the MXene-LNF membranes to remove sodium sulfate from water was studied. Incorporating MXene sheets into polyamide membranes during interfacial polymerization had a noticeable impact on water flux and sodium sulfate rejection (Fig. 4). The unmodified PA-LNF exhibited a water flux of 49.8 ± 6.0 LMH. By adding 0.04 wt% and 0.1 wt% MXene to the selective layer of the membranes, an elevated water flux of 59.1 ± 6.5 LMH was obtained. Reduced surface roughness, as evidenced by AFM earlier (Fig. 3$g_{1–4}$), decreased the hydraulic resistance faced by the water passing through the membrane—the reduced resistance results in enhanced water flow of the MXene-modified membranes. Additionally, the minimized penetration of the aqueous monomer solution during interfacial polymerization, caused by the generated MXene interlayer (verified by TEM images, Fig. 3$f_{1–4}$), led to a uniform pore size distribution, which helped achieve high water flux. Increasing the MXene concentration to 0.5 wt% decreases the water flux slightly to 53.6 ± 8.0 LMH. Despite the positive impact of MXene on the uniformity of the membrane, the coverage of the 0.5 wt% MXene-LNF membrane pores by MXene sheets observed in the SEM image (Fig. 3e_5) enhanced the transport resistance against the passage of water molecules.

The PA-LNF membrane exhibited a high sodium sulfate rejection rate of 95.4 ± 3.0 % (Fig. 4b). Nevertheless, the addition of MXene to the membrane matrix resulted in reduced salt rejection rates. The rejection rate for the 0.04 wt% MXene-LNF membrane was 88.5 ± 4.8 %, which decreased to 82.3 ± 5.9 % and 70.1 ± 3.7 % for the 0.1 wt% and 0.5 wt % MXene-LNF membranes, respectively. This pattern suggests that while MXene incorporation may enhance water flux, it tends to compromise the membrane's salt rejection. By generation of the MXene interlayer, as shown in the TEM images (Fig. 3$f_{3–4}$), we anticipated higher salt rejection rates due to introducing a barrier to the salt ions passage. However, the creation of a uniform pore size distribution and less irregularity/tortuosity upon MXene addition to the membrane network has a more significant impact on the barrier effect of the MXene interlayer. This modification allows for easier passage of salt ions, resulting in lower salt rejection rates. As 0.04 wt% MXene-LNF membrane exhibited improved water flux with an acceptable salt rejection rate, this membrane was used for subsequent experiments.

To extend the application of the MXene-modified membranes, 0.04 wt% MXene-LNF membranes were used to remove organic molecules from a wastewater sample. Fig. 5 thoroughly evaluates the performance of PA-LNF and 0.04 wt% MXene-LNF membranes in treating caffeine-spiked wastewater effluent. Besides caffeine removal, the membrane's removal efficacy of dissolved organic carbon (DOC) was evaluated. The PA-LNF membrane had a water flux of 55.8 ± 5.9 LMH, while the 0.04 wt% MXene-LNF membrane had a higher water flux of 62.9 ± 5.5 LMH. The improved water flux of the MXene-modified membrane can be attributed to the uniform pore size distribution and smooth surface, as evidenced by the analyzed structure and topology of the membranes. Both membranes performed similarly for DOC removal, with the PA-LNF membrane achieving almost 77.7–79.3 % removal rates. Regarding caffeine removal, the PA-LNF membrane achieved 81.9 ± 5.9 %, whereas the 0.04 wt% MXene-LNF membrane reached 76.3 ± 8.2 %. Despite caffeine being larger than ions, the reduced irregularity and tortuosity in the membrane network due to MXene addition has a more significant impact than the barrier effect of the MXene interlayer. While the MXene-LNF membrane showed a slight reduction in contaminant removal, its higher water flux may offer advantages in scenarios where higher throughput is desired.

MXene-LNF's antibacterial properties, as demonstrated by *Escherichia coli* (*E. coli*) inhibition tests, add another layer of efficacy, making these membranes particularly suitable for applications where microbial contamination is a concern. Fig. 6 shows the antibacterial efficacy of the 0.04 wt% MXene-incorporated LNF against *E. coli* compared to PA-LNF membrane as the control. The PA-LNF membrane inhibited *E. coli* at a

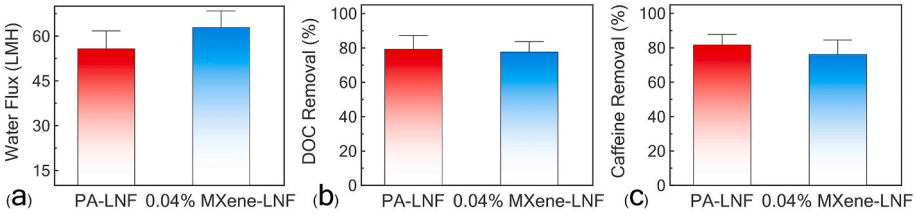

Fig. 5. The performance of PA-LNF and 0.04 wt% MXene-LNF membranes in treating a caffeine-spiked wastewater effluent were compared. The data show that the 0.04 wt% MXene-LNF membrane achieves a higher water flux of 62.9 ± 5.5 LMH than the PA-LNF membrane, which reaches 55.8 ± 5.9 LMH. While both membranes remove DOC at comparable rates, the PA-LNF membrane removes caffeine at a slightly higher rate. The figure emphasizes the trade-off between increased water flux and minor reductions in contaminant removal when MXene is incorporated into the membrane structure.

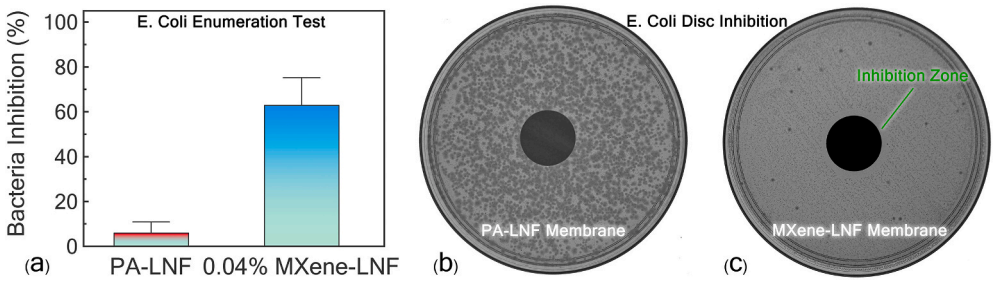

Fig. 6. The antibacterial efficacy of the unmodified polyamide LNF (PA-LNF) and 0.04 wt% MXene-LNF membranes against *E. coli* were compared. (a) The figure shows both the inhibition rates calculated relative to the control and the standard deviations used to assess the variability of the results. While the PA-LNF membrane inhibited *E. coli* at a poor and inconsistent rate of 6.1 % with a standard deviation of 4.8, the MXene-LNF membrane inhibited *E. coli* at a significantly higher rate of 63 %, albeit with a standard deviation of 12.2 (b and c). The figure also includes data from an inhibition zone assay, in which the MXene-LNF membrane demonstrated antibacterial activity by forming an inhibition zone on the agar plate, which the PA-LNF membrane did not. This multifaceted data presentation supports MXene-LNF's superior and more reliable antibacterial properties, arguing for its potential application in water treatment applications to reduce microbial contaminations.

modest 6.1 ± 4.8 % rate. This suggests poor antibacterial activity of the unmodified PA-LNF membrane. In contrast, the 0.04 wt% MXene-LNF membrane inhibited *E. coli* at a higher rate of 63.0 ± 12.2 %. Moderate antibacterial activity of the MXene-modified membrane is attributed to the low dispersion of MXene on the membrane surface, as evidenced by the TEM images. In addition to the standard enumeration agar plate test, an inhibition zone assay was performed to assess the membranes' antibacterial properties against *E. coli*. 0.04 wt% MXene-LNF membrane displayed a distinct inhibition zone on the agar plate, confirming its antibacterial efficacy. This zone of inhibition is a qualitative indicator of the membrane's ability to inhibit bacterial growth, and its presence validates the quantitative data from the enumeration test. On the other hand, the unmodified PA-LNF membrane failed to generate any inhibition zone, confirming its limited antibacterial activity. The formation of the inhibition zone in the MXene-LNF membrane but not in the PA-LNF membrane provides compelling evidence for the enhanced antimicrobial properties conferred by MXene incorporation, supporting its use in water treatment applications where microbial contamination is a concern.

3. Challenges and future prospect

The integration of MXenes possessing unique physicochemical properties into water treatment processes represents a promising strategy to advance this area by enhancing treatment efficiency and water quality. As a result of high water flux and decent rejection rates, MXene-LNF membranes are appealing options for biofiltration-membrane hybrid systems. While there is a trade-off regarding reduced salt and contaminant rejection, this concern is alleviated by the advantages of a hybrid system, where the biofiltration stage can handle a large portion of the contaminant removal. Future research should concentrate on harnessing the potential of MXenes in these hybrid systems. Various interdisciplinary sciences and technologies should be combined to optimize MXene-based LNF membranes to enhance membrane performance and address challenges such as long-term stability. In addition, further research and testing are vital to establish the scalability and capability of MXene-enhanced systems in real water treatment scenarios on large scales. Finally, to ensure sustainable and cost-effective implementation, a careful evaluation of the environmental and economic impacts of using MXenes in large-scale water treatment is necessary. When combined with biofiltration in a hybrid system, MXene-LNF membranes contribute to the evolving fields of both biofiltration and membrane systems, advancing the efficacy, sustainability, and cost-effectiveness of water treatment technologies. With ongoing research and development, these systems have the potential to substantially improve water reuse efforts, contributing to developing more effective and sustainable solutions for addressing the global water crisis.

In addition to enhanced water flux in LNF systems combined with biofiltration, the emphasis frequently shifts from high rejection rates to other operational efficiencies, such as antifouling capabilities. In this case, the antifouling properties of membranes are especially important. Membranes with improved antifouling properties can supplement the biofiltration stage's contaminant removal while maintaining high water flux and system reliability, making them ideal for biofiltration-nanofiltration hybrid systems. In this case, the effective antibacterial properties of MXenes add another layer of functionality to MXene-based LNF membranes, which is extremely useful in this context. Since biofouling is a common issue in membrane-based water treatment systems, the significant bacteria inhibition rates demonstrated by MXene-LNF membranes suggest that they may mitigate biofouling more effectively than conventional membranes.

We experimentally validate the effectiveness of MXenes in enhancing membrane performance and antibacterial properties without compromising the contaminant removal efficiency. Our experimental findings reveal that MXene-induced changes in morphology, topology, and structure of PA-LNF membranes upon its incorporation in the aqueous solution during interfacial polymerization, influencing water flux, contaminant rejection rates, and antibacterial activities. Enhanced water flux particularly at 0.04 wt% MXene concentration and antibacterial activities without a considerable decrease in pollutant removal efficiencies are aligned with the change in the morphology, topology, and structure, evidenced by SEM, AFM, TEM, and bacterial resistance results. The significant *E. coli* inhibition rates demonstrated by our MXene-PA-LNF membranes suggest that they may mitigate biofouling more effectively than conventional membranes. Looking ahead, research and dynamic experiments will be crucial to fully harness the potential of MXenes for decreasing fouling and biofouling of PA-LNF membranes. The experimental results show that MXene-LNF membranes have distinct advantages that make them particularly well-suited for use in biofiltration-membrane hybrid systems for advanced water reuse treatment.

Declaration of competing interest

The authors declare that they have no known competing financial interests or personal relationships that could have appeared to influence the work reported in this paper.

Acknowledgment

The authors wish to acknowledge partial funding through the National Science Foundation Established Program to Stimulate Competitive Research projects Grant RII Track 2 (# 2019561) and Grant RII Track 4 (# 2228903). This publication has not been formally reviewed

by NSF. The views expressed in this publication are solely those of authors and do not necessarily reflect those of NSF. Also, this research benefitted greatly from funding provided by USDATAT-RWTS 00-69526, USEPA Cooperative Agreement MX-00D87019, The Richard Lounsbery Foundation, and the Transforming Wastewater Infrastructure in the United States project of Columbia World Projects. This paper has not been formally reviewed by USDA or others agencies, and the views expressed in this document are solely those of the authors and do not necessarily reflect those of agencies.

Appendix A. Supplementary data

Supplementary data to this article can be found online at https://doi.org/10.1016/j.desal.2024.118198.

Data availability

Data will be made available on request.

References

[1] M.D. Firouzjaei, et al., Recent advances in functionalized polymer membranes for biofouling control and mitigation in forward osmosis, J. Membr. Sci. 596 (2020) 117604.
[2] T. Horseman, et al., Wetting, scaling, and fouling in membrane distillation: state-of-the-art insights on fundamental mechanisms and mitigation strategies, ACS ES&T Engineering 1 (1) (2020) 117–140.
[3] J.P. Chen, S. Kim, Y.-P. Ting, Optimization of membrane physical and chemical cleaning by a statistically designed approach, J. Membr. Sci. 219 (1–2) (2003) 27–45.
[4] S. Park, et al., Application of physical and chemical enhanced backwashing to reduce membrane fouling in the water treatment process using ceramic membranes, Membranes 8 (4) (2018) 110.
[5] B.F. Jirjis, S. Luque, Practical aspects of membrane system design in food and bioprocessing applications, in: Membrane Technology, Elsevier, 2010, pp. 179–212.
[6] M. Qasim, et al., The use of ultrasound to mitigate membrane fouling in desalination and water treatment, Desalination 443 (2018) 143–164.
[7] W.S. Ang, S. Lee, M. Elimelech, Chemical and physical aspects of cleaning of organic-fouled reverse osmosis membranes, J. Membr. Sci. 272 (1–2) (2006) 198–210.
[8] P. Goh, et al., Membrane fouling in desalination and its mitigation strategies, Desalination 425 (2018) 130–155.
[9] M. Pejman, et al., Improved antifouling and antibacterial properties of forward osmosis membranes through surface modification with zwitterions and silver-based metal organic frameworks, J. Membr. Sci. 611 (2020) 118352.
[10] D.Y. Zhang, et al., Antifouling polyimide membrane with grafted silver nanoparticles and zwitterion, Sep. Purif. Technol. 192 (2018) 230–239.
[11] N. Shahkaramipour, et al., Maximizing the grafting of zwitterions onto the surface of ultrafiltration membranes to improve antifouling properties, J. Membr. Sci. 601 (2020) 117909.
[12] D. Rana, T. Matsuura, Surface modifications for antifouling membranes, Chem. Rev. 110 (4) (2010) 2448–2471.
[13] H. Jafarian, et al., Synthesis of heterogeneous metal organic Framework-Graphene oxide nanocomposite membranes for water treatment, Chem. Eng. J. 455 (2023) 140851.
[14] M. Pejman, et al., In situ Ag-MOF growth on pre-grafted zwitterions imparts outstanding antifouling properties to forward osmosis membranes, ACS Appl. Mater. Interfaces 12 (32) (2020) 36287–36300.
[15] R. Kumar, A. Ismail, Fouling control on microfiltration/ultrafiltration membranes: effects of morphology, hydrophilicity, and charge, J. Appl. Polym. Sci. 132 (21) (2015).
[16] S.F. Anis, R. Hashaikeh, N. Hilal, Reverse osmosis pretreatment technologies and future trends: a comprehensive review, Desalination 452 (2019) 159–195.
[17] X. Zheng, Major Organic Foulants in Ultrafiltration of Treated Domestic Wastewater and their Removal by Bio-filtration as Pre-treatment, Papierflieger, 2010.
[18] O.D. Basu, S. Dhawan, K. Black, Applications of biofiltration in drinking water treatment–a review, J. Chem. Technol. Biotechnol. 91 (3) (2016) 585–595.
[19] F. Persson, et al., Performance of direct biofiltration of surface water for reduction of biodegradable organic matter and biofilm formation potential, Environ. Technol. 27 (9) (2006) 1037–1045.
[20] M. Vines, L.G. Terry, Removal of haloacetic acids via adsorption and biodegradation in a bench-scale filtration system, Water 15 (8) (2023) 1445.
[21] L.G. Terry, R.S. Summers, Biodegradable organic matter and rapid-rate biofilter performance: a review, Water Res. 128 (2018) 234–245.
[22] N. Moona, et al., Full-scale manipulation of the empty bed contact time to optimize dissolved organic matter removal by drinking water biofilters, ACS ES&T Water 1 (5) (2021) 1117–1126.
[23] A. Piche, et al., Investigation of backwash strategy on headloss development and particle release in drinking water biofiltration, Journal of Water Process Engineering 32 (2019) 100895.
[24] D.M. Moll, et al., Impact of temperature on drinking water biofilter performance and microbial community structure, Environ. Sci. Technol. 33 (14) (1999) 2377–2382.
[25] E.S. Peterson, R.S. Summers, Removal of effluent organic matter with biofiltration for potable reuse: a review and meta-analysis, Water Res. 199 (2021) 117180.
[26] H.A. Hasan, M.H. Muhammad, A review of biological drinking water treatment technologies for contaminants removal from polluted water resources, Journal of Water Process Engineering 33 (2020) 101035.
[27] N. Akbar, H. Aziz, M. Adlan, The characteristics of limestone and anthracite coal as filter media in treating pollutants from groundwater, Int. J. Environ. Sci. Dev. 12 (2) (2021) 58–62.
[28] Z.Z. Loh, et al., Shifting from conventional to organic filter media in wastewater biofiltration treatment: a review, Appl. Sci. 11 (18) (2021) 8650.
[29] W. Qin, et al., Nano manganese dioxide coupling carbon source preloading granular activated carbon biofilter enhancing biofilm formation and pollutant removal, Environ. Res. 241 (2024) 117606.
[30] A. Cescon, J.-Q. Jiang, Filtration process and alternative filter media material in water treatment, Water 12 (12) (2020) 3377.
[31] Y. Jeon, et al., Current understanding on biological filtration for the removal of microcystins, Chemosphere 313 (2023) 137160.
[32] M. Rattier, et al., Removal of micropollutants during tertiary wastewater treatment by biofiltration: role of nitrifiers and removal mechanisms, Water Res. 54 (2014) 89–99.
[33] Y. Zhao, et al., Insights into biofilm carriers for biological wastewater treatment processes: current state-of-the-art, challenges, and opportunities, Bioresour. Technol. 288 (2019) 121619.
[34] S. Velten, et al., Development of biomass in a drinking water granular active carbon (GAC) filter, Water Res. 45 (19) (2011) 6347–6354.
[35] A. Betsholtz, et al., New perspectives on the interactions between adsorption and degradation of organic m-icropollutants in granular activated carbon filters, Environ. Sci. Technol. 55 (2024) 11318–11327.
[36] Division, U.S.E.P.A.O.o.W.M.M.S., N.R.M.R.L.T. Transfer, and S. Division, Guidelines for Water Reuse. 2004: US Environmental Protection Agency.
[37] C. SWRCB, Regulations Related to Recycled Water, 2018.
[38] Commission, F.P.R, Framework for the Implementation of Potable Reuse in Florida, Published by the WateReuse Association, Alexandria, VA, Prepared for Florida Potable Reuse Commission, 2020.
[39] P.M. Huck, et al., Assessing the performance of biological filtration as pretreatment to low pressure membranes for drinking water, Environ. Sci. Technol. 43 (10) (2009) 3878–3884.
[40] C. Stoquart, et al., Hybrid membrane processes using activated carbon treatment for drinking water: a review, J. Membr. Sci. 411 (2012) 1–12.
[41] T. Nguyen, F.A. Roddick, L. Fan, Biofouling of water treatment membranes: a review of the underlying causes, monitoring techniques and control measures, Membranes 2 (4) (2012) 804–840.
[42] N.R. Maddela, et al., Biofouling in membrane bioreactors—mitigation and current status: a review, Appl. Biochem. Biotechnol. 195 (9) (2023) 5643–5668.
[43] M. Dadashi Firouzjaei, et al., MXenes: the two-dimensional influencers, Materials Today Advances 13 (2022) 100202.
[44] M. Naguib, et al., Two-dimensional nanocrystals produced by exfoliation of Ti3AlC2, Adv. Mater. 23 (37) (2011) 4248–4253.
[45] M. Sokol, et al., On the chemical diversity of the MAX phases, Trends in Chemistry 1 (2) (2019) 210–223.
[46] A. VahidMohammadi, J. Rosen, Y. Gogotsi, The world of two-dimensional carbides and nitrides (MXenes), Science 372 (6547) (2021) eabf1581.
[47] A. Grube, et al., Wearable textile supercapacitors: material advancements and applications, Journal of Energy Storage 99 (2024) 113228.
[48] S.S. Ray, et al., Towards the next generation improved throughput MXene-based membrane for environmental applications: a holistic review, J. Environ. Chem. Eng. 11 (3) (2023) 110243.
[49] M. Naguib, M.W. Barsoum, Y. Gogotsi, Ten years of progress in the synthesis and development of MXenes, Adv. Mater. 33 (39) (2021) 2103393.
[50] T. Li, et al., Fluorine-free synthesis of high-purity Ti3C2Tx (T= OH, O) via alkali treatment, Angew. Chem. Int. Ed. 57 (21) (2018) 6115–6119.
[51] Y. Wei, et al., Advances in the synthesis of 2D MXenes, Adv. Mater. 33 (39) (2021) 2103148.
[52] C. Zhou, et al., A review of etching methods of MXene and applications of MXene conductive hydrogels, Eur. Polym. J. 167 (2022) 111063.
[53] K. Arole, et al., Water-dispersible Ti3C2Tz MXene nanosheets by molten salt etching, Iscience 24 (12) (2021).
[54] K.R.G. Lim, et al., Fundamentals of MXene synthesis, Nature Synthesis 1 (8) (2022) 601–614.
[55] B. Anasori, Y. Gogotsi, MXenes: trends, growth, and future directions, Graphene 2D Mater. 7 (3–4) (2022) 75–79.
[56] M. Dadashi Firouzjaei, et al., Life-cycle assessment of Ti3C2Tx MXene synthesis, Adv. Mater. 35 (31) (2023) 2300422.
[57] H. Alyasi, et al., The power of MXene-based materials for emerging contaminant removal from water-a review, Desalination 566 (2024) 117913.
[58] F. Dixit, et al., Application of MXenes for water treatment and energy-efficient desalination: a review, J. Hazard. Mater. 423 (2022) 127050.
[59] M. Sajid, MXenes: are they emerging materials for analytical chemistry applications?–a review, Anal. Chim. Acta 1143 (2021) 267–280.

[60] M.N.H. Rozaini, et al., Potential application of 2D nano-layered MXene in analysing and remediating endocrine disruptor compounds and heavy metals in water, Environ. Geochem. Health 46 (3) (2024) 111.
[61] A. Thakur, et al., Step-by-step guide for synthesis and delamination of Ti3C2Tx MXene, Small, Methods 7 (2023) 2300030.
[62] Z. Ling, et al., Flexible and conductive MXene films and nanocomposites with high capacitance, Proc. Natl. Acad. Sci. 111 (47) (2014) 16676–16681.
[63] H.T.A. Awan, et al., MXene-polymer hybrid composites for advanced energy storage: insights into supercapacitors and batteries, Journal of Energy Storage 95 (2024) 112449.
[64] T. Rasheed, et al., Cutting-edge developments in MXene-derived functional hybrid nanostructures: a promising frontier for next-generation water purification membranes, Chemosphere 357 (2024) 141955.
[65] Z. Zandi, et al., Electro-conductive Ti3C2 MXene multilayered membranes: dye removal and antifouling performance, Adv. Funct. Mater. 34 (36) (2024) 2401970.
[66] S. Ye, et al., MXene: a wonderful nanomaterial in antibacterial, Front. Bioeng. Biotechnol. 12 (2024) 1338539.
[67] K. Fu, et al., Highly efficient and selective Hg (II) removal from water using multilayered Ti3C2O x MXene via adsorption coupled with catalytic reduction mechanism, Environ. Sci. Technol. 54 (24) (2020) 16212–16220.
[68] A. Lipatov, et al., Elastic properties of 2D Ti3C2T x MXene monolayers and bilayers, Sci. Adv. 4 (6) (2018) eaat0491.
[69] A. Prasad, et al., Mechanical behavior of MXene-polymer layered nanocomposite using computational finite element analysis, Compos. Part B Eng. 284 (2024) 111689.
[70] Y. Li, et al., Aramid nanofiber membranes reinforced by MXene nanosheets for recovery of dyes from textile wastewater, ACS Applied Nano Materials 4 (6) (2021) 6328–6336.
[71] J. Ma, et al., MXene (Ti3T2CX)-reinforced thin-film polyamide nanofiltration membrane for short-chain perfluorinated compounds removal, Process. Saf. Environ. Prot. 168 (2022) 275–284.
[72] N. Dwivedi, et al., Emergent 2D materials for combating infectious diseases: the potential of MXenes and MXene–graphene composites to fight against pandemics, Materials Advances 2 (9) (2021) 2892–2905.
[73] F. Seidi, et al., MXenes antibacterial properties and applications: a review and perspective, Small 19 (14) (2023) 2206716.
[74] A. Arabi Shamsabadi, et al., Antimicrobial mode-of-action of colloidal Ti3C2T x MXene nanosheets, ACS Sustain. Chem. Eng. 6 (12) (2018) 16586–16596.
[75] K. Rasool, et al., Water treatment and environmental remediation applications of two-dimensional metal carbides (MXenes), Mater. Today 30 (2019) 80–102.
[76] S.S. Siwal, et al., Novel synthesis methods and applications of MXene-based nanomaterials (MBNs) for hazardous pollutants degradation: future perspectives, Chemosphere 293 (2022) 133542.
[77] M. Bilal, U. Khan, I. Ihsanullah, MXenes: the emerging adsorbents for the removal of dyes from water, J. Mol. Liq. 385 (2023) 122377.
[78] X. Hu, et al., Kinetics, isotherm and chemical speciation analysis of Hg (II) adsorption over oxygen-containing MXene adsorbent, Chemosphere 278 (2021) 130206.
[79] P. Zhang, et al., Novel two-dimensional magnetic titanium carbide for methylene blue removal over a wide pH range: insight into removal performance and mechanism, ACS Appl. Mater. Interfaces 11 (27) (2019) 24027–24036.
[80] S. Nezami, A. Ghaemi, T. Yousefi, Application of titanium carbide/nitride (MXene)-based NPs in adsorption of radionuclides and heavy metal ions for wastewater remediation: a review, Case Studies in Chemical and Environmental Engineering 7 (2023) 100326.
[81] A.P. Isfahani, et al., Efficient mercury removal from aqueous solutions using carboxylated Ti3C2Tx MXene, J. Hazard. Mater. 434 (2022) 128780.
[82] D. Park, et al., Removal of selected contaminants of dyes and pharmaceuticals using MXene-based nanoadsorbents: a review, Sep. Purif. Technol. 341 (2024) 126864.
[83] L. Wang, et al., Rational control of the interlayer space inside two-dimensional titanium carbides for highly efficient uranium removal and imprisonment, Chem. Commun. 53 (89) (2017) 12084–12087.
[84] A. Shahzad, et al., Two-dimensional Ti3C2T x MXene nanosheets for efficient copper removal from water, ACS Sustain. Chem. Eng. 5 (12) (2017) 11481–11488.
[85] A.K. Fard, et al., Barium removal from synthetic natural and produced water using MXene as two dimensional (2-D) nanosheet adsorbent, Chem. Eng. J. 317 (2017) 331–342.
[86] W. Mu, et al., Improving barium ion adsorption on two-dimensional titanium carbide by surface modification, Dalton Trans. 47 (25) (2018) 8375–8381.
[87] G. Zou, et al., Synthesis of urchin-like rutile titania carbon nanocomposites by iron-facilitated phase transformation of MXene for environmental remediation, J. Mater. Chem. A 4 (2) (2016) 489–499.
[88] Y. Dong, et al., Mxene/alginate composites for lead and copper ion removal from aqueous solutions, RSC Adv. 9 (50) (2019) 29015–29022.
[89] S. Li, et al., Efficient thorium (IV) removal by two-dimensional Ti2CTx MXene from aqueous solution, Chem. Eng. J. 366 (2019) 192–199.
[90] A.R. Khan, et al., Two-dimensional transition metal carbide (Ti 3 C 2 T x) as an efficient adsorbent to remove cesium (Cs+), Dalton Trans. 48 (31) (2019) 11803–11812.
[91] A. Shahzad, et al., Mercuric ion capturing by recoverable titanium carbide magnetic nanocomposite, J. Hazard. Mater. 344 (2018) 811–818.
[92] P. Zhang, et al., Sorption of Eu (III) on MXene-derived titanate structures: the effect of nano-confined space, Chem. Eng. J. 370 (2019) 1200–1209.
[93] Y. Ying, et al., Two-dimensional titanium carbide for efficiently reductive removal of highly toxic chromium (VI) from water, ACS Appl. Mater. Interfaces 7 (3) (2015) 1795–1803.
[94] A. Shahzad, et al., Exfoliation of titanium aluminum carbide (211 MAX phase) to form nanofibers and two-dimensional nanosheets and their application in aqueous-phase cadmium sequestration, ACS Appl. Mater. Interfaces 11 (21) (2019) 19156–19166.
[95] P. Gu, et al., Experimental and theoretical calculation investigation on efficient Pb (II) adsorption on etched Ti 3 AlC 2 nanofibers and nanosheets, Environ. Sci. Nano 5 (4) (2018) 946–955.
[96] W. Mu, et al., Removal of radioactive palladium based on novel 2D titanium carbides, Chem. Eng. J. 358 (2019) 283–290.
[97] Y. Tang, C. Yang, W. Que, A novel two-dimensional accordion-like titanium carbide (MXene) for adsorption of Cr (VI) from aqueous solution, J. Adv. Dielectr. 8 (05) (2018) 1850035.
[98] A. Shahzad, et al., Ti3C2Tx MXene core-shell spheres for ultrahigh removal of mercuric ions, Chem. Eng. J. 368 (2019) 400–408.
[99] L. Wang, et al., Effective removal of anionic Re (VII) by surface-modified Ti2CT x MXene nanocomposites: implications for Tc (VII) sequestration, Environ. Sci. Technol. 53 (7) (2019) 3739–3747.
[100] L. Wang, et al., Efficient U (VI) reduction and sequestration by Ti2CT x MXene, Environ. Sci. Technol. 52 (18) (2018) 10748–10756.
[101] L. Wang, et al., Loading actinides in multilayered structures for nuclear waste treatment: the first case study of uranium capture with vanadium carbide MXene, ACS Appl. Mater. Interfaces 8 (25) (2016) 16396–16403.
[102] B.-M. Jun, et al., Adsorption of selected dyes on Ti3C2Tx MXene and Al-based metal-organic framework, Ceram. Int. 46 (3) (2020) 2960–2968.
[103] F. Meng, et al., MXene sorbents for removal of urea from dialysate: a step toward the wearable artificial kidney, ACS Nano 12 (10) (2018) 10518–10528.
[104] N. Maroufi, N. Hajilary, Nanofiltration membranes types and application in water treatment: a review, Sustainable Water Resources Management 9 (5) (2023) 142.
[105] A.A. Khan, S. Boddu, Hybrid membrane process: an emerging and promising technique toward industrial wastewater treatment, in: Membrane-based Hybrid Processes for Wastewater Treatment, Elsevier, 2021, pp. 257–277.
[106] T. Zhang, et al., Loose nanofiltration membranes for selective rejection of natural organic matter and mineral salts in drinking water treatment, J. Membr. Sci. 662 (2022) 120970.
[107] E.M. Vrijenhoek, J.J. Waypa, Arsenic removal from drinking water by a "loose" nanofiltration membrane, Desalination 130 (3) (2000) 265–277.
[108] X. Feng, et al., Recent advances of loose nanofiltration membranes for dye/salt separation, Sep. Purif. Technol. 285 (2022) 120228.
[109] S. Mohammad Nejad, et al., Loose nanofiltration membranes functionalized with in situ-synthesized metal organic framework for water treatment, Materials Today Chemistry 24 (2022) 100909.
[110] P. Kong, et al., Advances in the application of graphene oxide composite loose nanofiltration membranes for dye and salt separation, J. Environ. Chem. Eng. 12 (2024) 114278.
[111] P. Jin, et al., Loose nanofiltration membranes for the treatment of textile wastewater: a review, Journal of Membrane Science and Research 8 (3) (2022).
[112] Rahimpour, A., et al., Chapter 1 - nonsolvent-induced phase separation, in Polymeric Membrane Formation by Phase Inversion, N. Tavajohi and M. Khayet, Editors. 2024, Elsevier. p. 1–36.
[113] N. Khatoon, et al., Review of MOFs and their applications in the preparation of loose nanofiltration membranes for dye and salt fractionation, Desalin. Water Treat. 317 (2024) 100092.
[114] S.A. Aktij, et al., Metal-organic frameworks' latent potential as high-efficiency osmotic power generators in thin-film nanocomposite membranes, Chem. Eng. J. 481 (2024) 148384.
[115] M. Paul, S.D. Jons, Chemistry and fabrication of polymeric nanofiltration membranes: a review, Polymer 103 (2016) 417–456.
[116] B. Sutariya, S. Karan, A realistic approach for determining the pore size distribution of nanofiltration membranes, Sep. Purif. Technol. 293 (2022) 121096.
[117] X. Li, et al., Regulating the interfacial polymerization process toward high-performance polyamide thin-film composite reverse osmosis and nanofiltration membranes: a review, J. Membr. Sci. 640 (2021) 119765.
[118] M.Q. Seah, et al., Progress of interfacial polymerization techniques for polyamide thin film (nano) composite membrane fabrication: a comprehensive review, Polymers 12 (12) (2020) 2817.
[119] Y.A. Al-Hamadani, et al., Applications of MXene-based membranes in water purification: a review, Chemosphere 254 (2020) 126821.
[120] R.R. Choudhury, et al., Antifouling, fouling release and antimicrobial materials for surface modification of reverse osmosis and nanofiltration membranes, J. Mater. Chem. A 6 (2) (2018) 313–333.
[121] Q. Xue, K. Zhang, The preparation of high-performance and stable MXene nanofiltration membranes with MXene embedded in the organic phase, Membranes 12 (1) (2021) 2.
[122] R. Akhter, S.S. Maktedar, MXenes: Acomprehensive review of synthesis, properties, and progress in supercapacitor applications, J. Mater. 9 (2023) 1196–1241.
[123] M.A. Naji, et al., Novel mxene-modified polyphenyl sulfone membranes for functional nanofiltration of heavy metals-containing wastewater, Membranes 13 (3) (2023) 357.
[124] X. Yang, et al., Construction of Fe3O4@ MXene composite nanofiltration membrane for heavy metal ions removal from wastewater, Polym. Adv. Technol. 32 (3) (2021) 1000–1010.

[125] R. Ghanbari, et al., Ti3C2Tx MXene@ MOF decorated polyvinylidene fluoride membrane for the remediation of heavy metals ions and desalination, Chemosphere 311 (2023) 137191.
[126] S. Wang, et al., Removal of heavy metal cations and co-existing anions in simulated wastewater by two separated hydroxylated MXene membranes under an external voltage, J. Membr. Sci. 638 (2021) 119697.
[127] I. Mahar, et al., Fabrication and characterization of MXene/carbon composite-based nanofibers (MXene/CNFs) membrane: an efficient adsorbent material for removal of Pb+ 2 and As+ 3 ions from water, Chem. Eng. Res. Des. 191 (2023) 462–471.
[128] T.-Q. Zhang, et al., Exfoliated MXene/poly-melamine-formaldehyde composite membranes for removal of heavy metals and organics from aqueous solutions, J. Hazard. Mater. 463 (2024) 132866.
[129] Z. Xu, et al., Assembly of 2D MXene nanosheets and TiO2 nanoparticles for fabricating mesoporous TiO2-MXene membranes, J. Membr. Sci. 564 (2018) 35–43.
[130] Q. Long, et al., Self-assembly enabled nano-intercalation for stable high-performance MXene membranes, J. Membr. Sci. 635 (2021) 119464.
[131] D.-D. Shao, et al., Enhancing interfacial adhesion of MXene nanofiltration membranes via pillaring carbon nanotubes for pressure and solvent stable molecular sieving, J. Membr. Sci. 623 (2021) 119033.
[132] S. Wei, et al., Two-dimensional graphene oxide/MXene composite lamellar membranes for efficient solvent permeation and molecular separation, J. Membr. Sci. 582 (2019) 414–422.
[133] T. Liu, et al., Two-dimensional MXene incorporated graphene oxide composite membrane with enhanced water purification performance, J. Membr. Sci. 593 (2020) 117431.
[134] G. Zeng, et al., High-performing composite membrane based on dopamine-functionalized graphene oxide incorporated two-dimensional MXene nanosheets for water purification, J. Mater. Sci. 56 (2021) 6814–6829.
[135] C.E. Ren, et al., Charge-and size-selective ion sieving through Ti3C2T x MXene membranes, The journal of physical chemistry letters 6 (20) (2015) 4026–4031.
[136] M. Dadashi Firouzjaei, et al., Functionalized polyamide membranes yield suppression of biofilm and planktonic bacteria while retaining flux and selectivity, Sep. Purif. Technol. 282 (2022) 119981.
[137] H.E. Karahan, et al., MXene materials for designing advanced separation membranes, Adv. Mater. 32 (29) (2020) 1906697.
[138] A. Lipatov, et al., Effect of synthesis on quality, electronic properties and environmental stability of individual monolayer Ti3C2 MXene flakes, Advanced Electronic Materials 2 (12) (2016) 1600255.
[139] L. Zhao, et al., A new method for modeling rough membrane surface and calculation of interfacial interactions, Bioresour. Technol. 200 (2016) 451–457.
[140] L. Chen, et al., Interaction energy evaluation of soluble microbial products (SMP) on different membrane surfaces: role of the reconstructed membrane topology, Water Res. 46 (8) (2012) 2693–2704.